Introduction

Many engineering problems require accurate estimates of stress and strain conditions. Measurements of bedrock and overburden shear-wave velocities allow reasonable approximations to be made for key modulus. Elastic moduli are essential material characteristics when describing and modelling a volume of earth for engineering applications. Shear-wave velocities can be estimated using several different seismic surface-wave methods. One of the most recent advances in the surface-wave analysis include multichannel analysis of surface-wave (MASW) method, developed to estimate near-surface S-wave velocity from high-frequency (≥ 2 Hz) Rayleigh-wave data (Miller et al., 1999, Song et al., 1989, Park et al., 1998, Xia et al., 1999). The MASW method originally focused on and was developed around active (human controlled) seismic sources. It was later expanded to use passive seismic sources (Park et al. 2004). Passive surface waves generated from ambient noise (mainly vehicle traffic) are generally low frequency and can have wavelengths that reach tens to hundreds of meters (Okada, 2003). The passive surface wave method therefore has the potential to reach investigation depths significantly greater than active sources and can be effectively used in very noisy settings.

Using a passive source dramatically reduces the control over parameters like angle of incoming wave, distance and number of sources and source wavelet timing become unknown and consequently a 1D array of receivers is not adequate. A 2D array is necessary at most sites to extract a realistic dispersion trend (Park et al. 2007). Furthermore a relatively large spread layout and a reasonably significant distance from the passive source is necessary to allow the plane waves to fully develop.

In this study the optimal spread layout and orientation is investigated and determined that would allow surface wave penetration deep enough into the bedrock to permit studies of stress and strain conditions at the bedrock surface.

Data processing

Data have been processed using the dispersion imaging scheme described by Park et al. (2004). For this method the processing scheme for a 2D layout had to evolve by extending the 1D approach described by Park et al. (1998). In the 2D- case, the azimuths of the two scanning parameters (frequency and phase velocity) of the incoming surface wave were added: a particular frequency of surface wave energy is plotted in a phase velocity-azimuth diagram. The energy is then stacked over all the azimuths. The stacked information for every scanned frequency results in the dispersion image. A detailed description can be found in Park et al. (2004).

Data acquisition

For this research study an array of 336 receivers was deployed in a 2-D spread (Figure 1d). The 4.5 Hz vertical geophones were orientated at parallel and orthogonal alignments to nearby railroad tracks in 7 WE-lines and 5 NS-lines. Ten of the twelve lines that made of the 2-D spread included 24 receivers with a receiver spacing of 2.5 m. Two of the lines were orthogonal and included 48 receivers at 1.2 m separations. The dominant energy source were trains travelling rails that passed both along the north and west sides of the site. By selecting the appropriate recording times it was possible to uniquely capture trains approaching or moving away from the spread from a wide range of azimuthal orientations. Each record was 32 sec long with a sample interval of 2 msec.

Study

The first and key step in processing these data was sorting out the records that had good broadband energy principally from one direction and then finding an adequate time window within those higher quality 32 sec records. The time section needed to be long enough to capture a representative segment of information, but short enough to constrain energy to a stable azimuth angle, -at least for the

frequencies of interest. Once the records and time windows were selected the data were processed following the scheme from Park et al. (1998 and 2004).

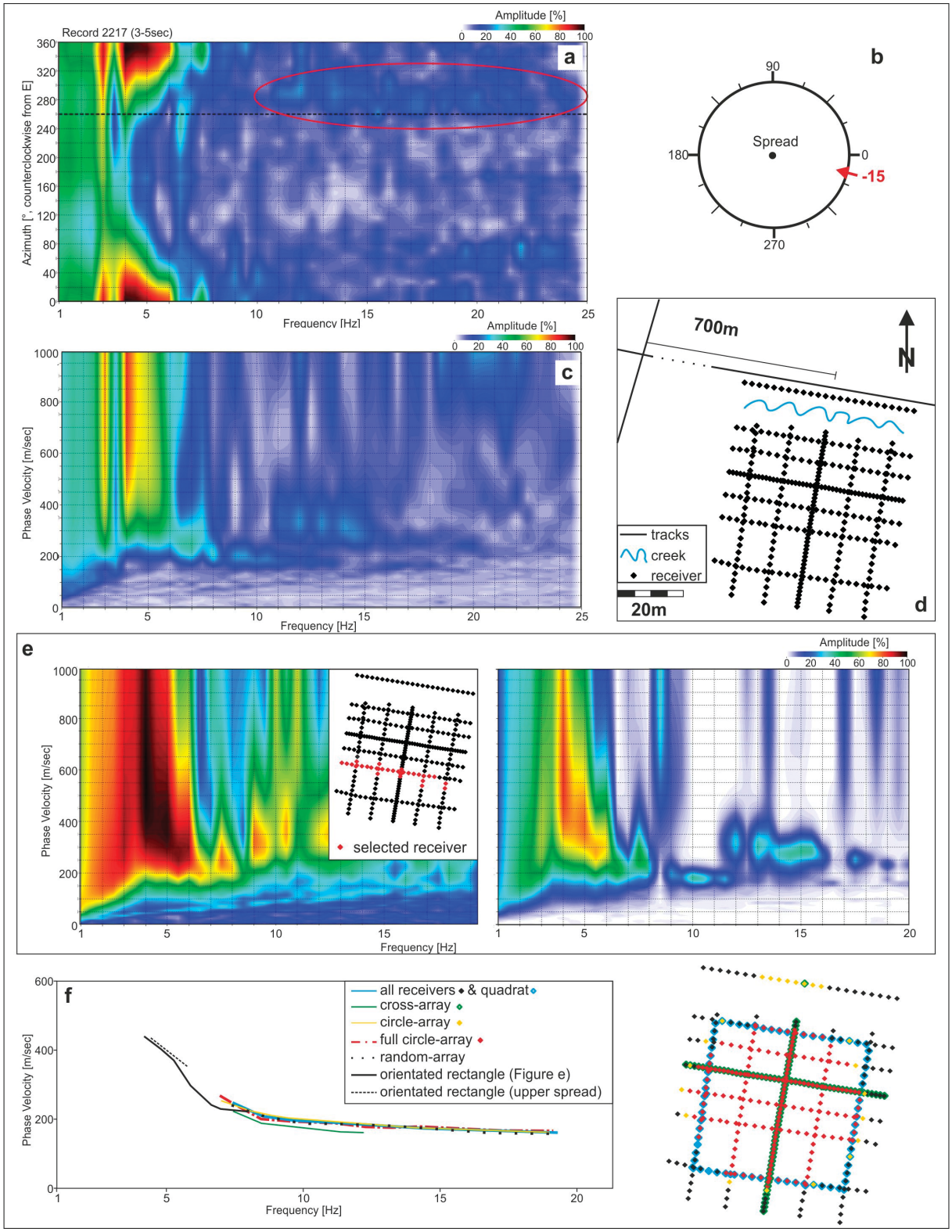

Figure 1 *a) Azimuth versus frequency diagram, black line margins the SE quadrant, red circle shows energy concentration in the higher frequencies, b) incoming wave direction (4-6Hz), c) Phase-velocity frequency image from the whole spread, d) receiver layout and surroundings, e) Phase-velocity frequency image from a rectangle orientated parallel to incoming waves, right: combined with high frequency improved array, f) dispersion curves of different arrays.*

The relatively large overall spread made it possible to compare various sub-arrays by processing only selected groups of receivers.

Example 1

The first example is a record where the main energy comes from a train travelling east; the back of the train is about 2.5 km east of the spread. In Figure 1a the Azimuth-Frequency diagram shows the main energy for frequencies from 4 to 6Hz at an angle of 345° (SE quadrant, Figure 1b). The higher frequencies accumulate mainly around 280° (see red circles Figure 1a). Figure 1c shows the energy distribution of the dispersion image, for the whole spread; according to the Azimuth-Frequency diagram, only the incoming surface waves from the SE quadrant are considered. The dispersion curve for the whole spread can be interpreted to a frequency of 6Hz, indicative of an approximate investigation depth of 22.5 meters (Xia et al. 1999).

For comparison, dispersion curves for different receiver arrays are calculated (Figure 1f). None of the spreads resolve frequencies higher than about 6 Hz.

Figure 2e displays a dispersion image calculated from a narrow rectangular array with 30 receivers and a width of 2 m and a length of 56.5 m, orientated as parallel as possible to the main energy of the incoming surface waves with frequencies between 4 and 6 Hz. These images allow picking a dispersion curve with defensible arrivals as low as 4 Hz, which relates to wavelengths that extend to an investigation depth of about 48 meters (Xia et al. 1999). As mentioned above the higher frequencies come from a different incident angle, so by using this method of array tuning and energy segregation a second image (Figure 1e (right)) can be produced that combines the low frequency dispersion curve with the high frequency dispersion curve calculates separately from different parts of the overall shot record and using a different tuned array. This approach dramatically increases the continuity of the dispersion curve for this site.

Figure 1f summarizes the dispersion-curve estimates obtained from various arrays. The curves from the different arrays covering only the higher frequencies are consistent. The two curves for the lower frequencies vary a bit from each other, a phenomenon that can be explained by the different position in the initial array. The crossover from the lower to the higher frequency curves is quite smooth. It has to be kept in mind that the higher frequency curves cover more or less the whole initial array, an area of around 4000 m^2, whereas the rectangles orientated to 345°SE cover only about 120 m^2.

Example 2

The second example is a record where the main energy comes from a train travelling west of the spread moving from South to North. The azimuthal frequency diagram (Figure 2a) from the selected time window shows an accumulation in the low-frequency part of the spectrum at about 150° (NW-quadrant, Figure 2b). The higher frequency energy is distributed (red eclipses) across other searching quadrants.

The energy distribution of the dispersion image for the whole spread,-according to Figure 2a, incoming waves from all directions are incorporated-,can be interpreted down to a frequency of 7 to 7.5Hz on these data (Figure 2d), which equates to an investigation depth of around 16 meters (Xia et al. 1999).

Processing a 2-D spread of geophones, laying in a 2 by 60 m array elongated towards 150° NW (Figure 2c), makes it possible to pick phase velocities on this images down to a frequency close to 4 Hz (Figure 2d). After Xia et al. (1999) this equates to a depth of about 51 meters.

Conclusions

If an array is orientated parallel to the direction of incident low frequency waves, it is possible to resolve frequencies as low as 4 Hz even using small number of receivers (from 20 on) These lower

frequencies allow a marked increase in the maximum depth of investigation, thereby, helping to solve engineering problems at greater depths than possible with active source investigations.

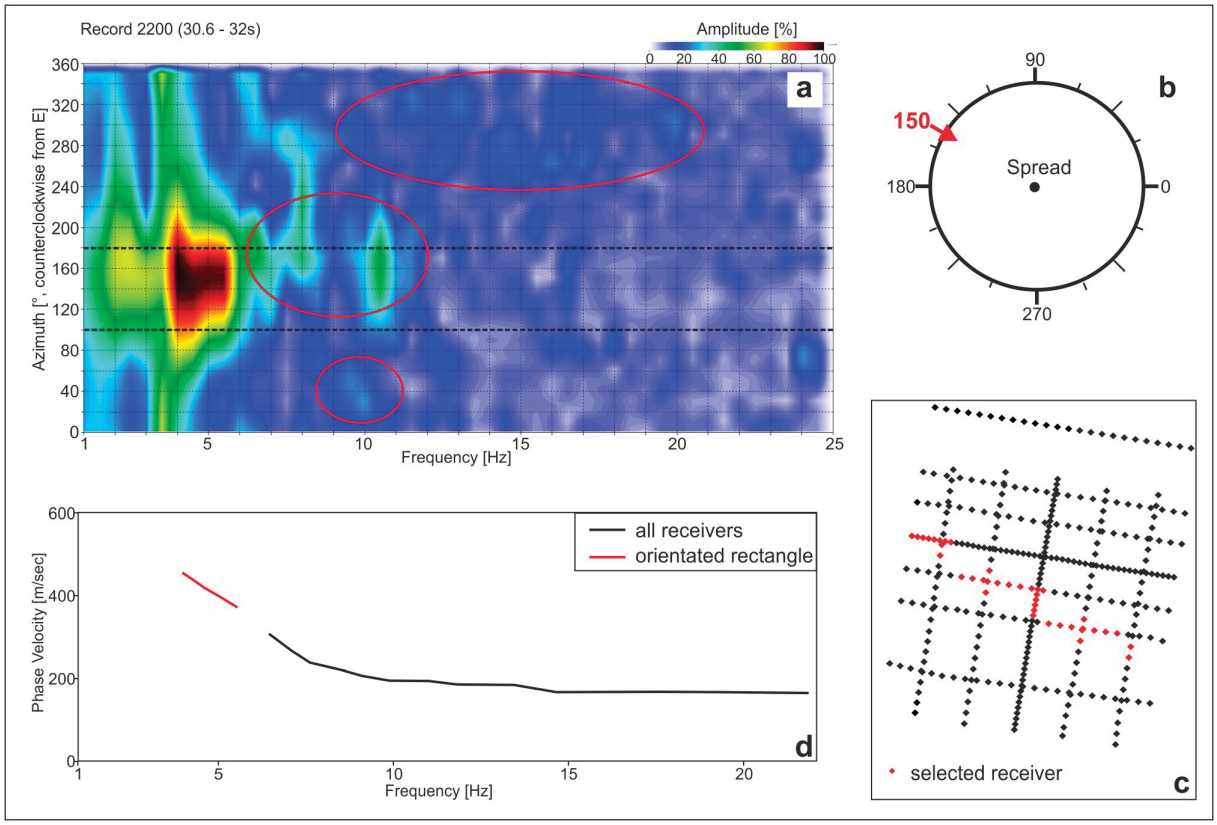

Figure 2 *a) Azimuth versus frequency diagram, black line margins the NW quadrant, red circles show energy concentration in the higher frequencies, b) incoming wave direction(4-5.5Hz), c) rectangle orientated parallel to incoming waves of low frequencies, d) dispersion curves of all receivers and of the orientated rectangle.*

References

Miller, R. D., Xia, J., Park, C. B., and Ivanov, J.M. [1999] Multichannel analysis of surfaces waves to map bedrock. *Leading Edge*, **18**, 1392-1396.

Okada, H. [2003] *The microtremor survey method*, Geophysical Monograph Series, **12**, SEG, Tulsa.

Park, C.B., Xia, J. and Miller, R.D. [1998] Imaging dispersion curves of surface wave s on multi-channel record. *SEG,* Extended Abstracts, 1377-1380.

Park, C., R. Miller, D. Laflen, N. Cabrillo, J. Ivanov, B. Bennett, and Huggins, R. [2004] Imaging dispersion curves of passive surface waves. *SEG,* Extended Abstracts, 1357-1360.

Park, C.B., Miller, R.D., and Xia, J and Ivanov, J. [2007] Multichannel analysis of surface waves (MASW)-active and passive methods. *Leading Edge*, **26**(1), 60-65.

Song, Y.Y., J.P. Castagna, R.A. Black, and Knapp, R.W. [1989] Sensitivity of near-surface shear-wave velocity determination from Rayleigh and Love waves. *SEG, 59th Annual Meeting, Dallas, Texas*, Technical Program with Biographies, 509-512.

Xia, J., Miller, R.D., and Park, C.B. [1999] Estimation of near surface shear-wave velocity by inversion of Rayleigh waves. *Geophysics*, **64**, 691-700.